Experimental Mechanics (2018) 58:847–858
https://doi.org/10.1007/s11340-018-0374-7

Experimental Study of the Effect of Temperature on Strength and Extensibility of Rubberlike Materials

Y. Lev[1] · A. Faye[1] · K. Y. Volokh[1]

Received: 14 August 2017 / Accepted: 18 January 2018 / Published online: 4 April 2018

Abstract

Rubber-like materials are widely used in several industrial applications. In these applications, rubber components are largely subjected to biaxial loading at a range of temperatures. In this work, we study the effect of short-term temperature on the ultimate properties of rubber materials, particularly, their strength. Such studies are lacking in the literature. For this purpose, we consider three different rubber-like materials; Nitrile Butadiene Rubber (NBR), Neoprene and Silicone. These rubber materials are tested under equi-biaxial tension using the bulge test. Tests are conducted till failure under a constant temperature. Four different temperatures are considered; 25 °C, 50 °C, 70 °C and 90 °C. Experiments are modeled using a finite element method. A constitutive model which includes the description of failure through energy limiters is calibrated against the bulge experiments. It is found that while the material stiffness is not significantly affected by temperature the ultimate stress and stretch, as well as the energy limiter for NBR and Neoprene greatly depend upon temperature. Stress carrying capacity for NBR and Neoprene decreases drastically at the highest temperature considered as compared to their values at room temperature (25 °C). Properties of Silicone are not affected significantly because of its temperature resistance. A new constitutive function is developed for the energy limiter, which allows unifying the description of different materials.

Keywords Strength · Rubber · Bulge test · Energy limiters · Temperature

Introduction

Rubber-like materials are widely used in industrial applications. In many cases such as vehicle tires and seals, rubber materials are subjected to a range of temperatures [1, 2]. We will show that temperature has a short-term effect on rubber materials. Thus it is required to characterize these materials to temperatures other than room temperature. The effect of temperature on mechanical properties of rubber-like materials have largely been studied from the stiffness point of view [2–7]. Experiments which focus on failure of rubber-like materials are mostly conducted at room temperature only [8–10]. The effect of temperature on ultimate strength and elongation for rubber materials is hard to find in the literature [11]. The large extension of elastomers makes it difficult to test inside a controlled temperature environment. Although uniaxial tests are routinely done with commercially load frames and environmental chambers, most are not able to reach the ultimate stretch values of about 7. In the present work, the effect of common high operating temperatures on the ultimate strength and elongation of elastomers is experimentally studied. The popular "bulge test" method (also known as the "inflation test" or "balloon test") is adopted here in order to characterize the mechanical behavior of rubber materials [9, 12–14]. The bulge test procedure involves inflation of a circular rubber sheet, clamped around its edges, by pressurized air under one of its faces. The bulge test has two main advantages compared to the uniaxial test; (1) The bulge test is relatively easy to perform under a temperature controlled environment by placing the whole test device inside a chamber. (2) The pole of the inflated sheet experiences equi-biaxial tension strain due to axial symmetry of the bulge test configuration. Rubber materials under many practical applications, such as tubes and membranes, are subjected to biaxial tension. Thus, bulge tests provides a better way to characterize materials for such applications [14].

✉ Y. Lev
yoavlevsmail@gmail.com

1 Faculty of Civil and Environmental Engineering, Technion, Israel

In the present work, three different rubber materials which are widely used in industrial applications are chosen for experiments. (a) Nitrile Butadiene Rubber (NBR), Sulfur vulcanized with Shore 41A, density of 1.141 gr/cm^3, and glass transition/melting temperature of −35 °C/100 °C. This rubber material can be significantly stretched, is resistant to oil, fuel and other chemicals [15], hence widely used in automotive and aeronautical industries to make fuel and oil handling hoses, seals, grommets and self-sealing fuel tanks. (b) Neoprene, Sulfur vulcanized with Shore 35A, a density of 1.33 gr/cm^3, and glass transition/melting temperature of −55 °C/100 °C. This rubber material has chemical resistance and it maintains flexibility over a wide temperature range. It is widely used as a load bearing base in civil industries [16]. (c) Silicone rubber, Peroxide vulcanized with Shore 41A, a density of 1.13 gr/cm^3, and glass transition/melting temperature of −60 °C/200 °C. It is best known for its resistance to temperature and extreme environments. Because of these properties, they are widely used in many applications, such as automotive, electronics and sportswear [17]. All 3 rubber materials are purchased from “GUMIAN rubber products LTD”.

Bulge experiments are performed at four different temperatures; 25 °C, 50 °C, 70 °C and 90 °C. All experiments are performed till failure. To characterize these materials, we use an appropriate constitutive model which can also model failure. Finite element (FE) simulations of bulge tests are performed and material stiffness and failure parameters are obtained as a function of temperature by comparison between experiments and simulations.

The rest of the paper is organized in the following manner: details of the experimental set-up for conducting bulge tests under a constant temperature environment are presented in “Experimental Setup”; results from the experiments are discussed in “Experiment Results”; the Constitutive model considered for characterization of the material and details of FE simulations are given in “Finite Element Modeling of the Bulge Test”; the procedure for calibration of the constitutive model to find the material parameters is discussed in “Calibration of the Constitutive Model”, including a suggested relation for a thermoelastic energy limiter theory; finally, summary and conclusion are presented in “Conclusions”.

Experimental Setup

The device for the bulge test is shown in Fig. 1(a). It consists of three metallic flanges bolted together. The top flange has a circular opening of 100 mm diameter with round corners. The bottom flange has several channels provided for instrumentation. The middle flange has an opening for air to inflate the rubber sheet by applying internal pressure. Square shaped specimens are cut from rubber sheets and clamped between the top and middle flanges. A schematic view of the bulge test is shown in Fig. 1(b). The set-up for conducting the bulge test at a constant temperature environment is shown in Fig. 2. The bulge test device is placed inside a chamber made of Polycarbonate sheets. Walls of the chamber are insulated from inside to prevent heat loss. The temperature inside the chamber is controlled using a hot-air blower with integrated temperature control. We add an additional design to the well established bulge test technique, allowing temperature control also inside the inflating balloon. This is done by using a very long (15 m) and narrow (inner diameter of 3.8 mm) tube. The tube is placed inside the chamber and is pre-heated together with the bulge device. Air flows slowly through the long and narrow pre-heated tube and by the time air inflates the balloon, temperatures inside and outside the balloon are almost the same. This is provided by the five thermocouples (T_1 to T_5) placed one at each wall of the chamber and one

a b

Fig. 1 (**a**) Bulge test device, (**b**) Schematic view of bulge test

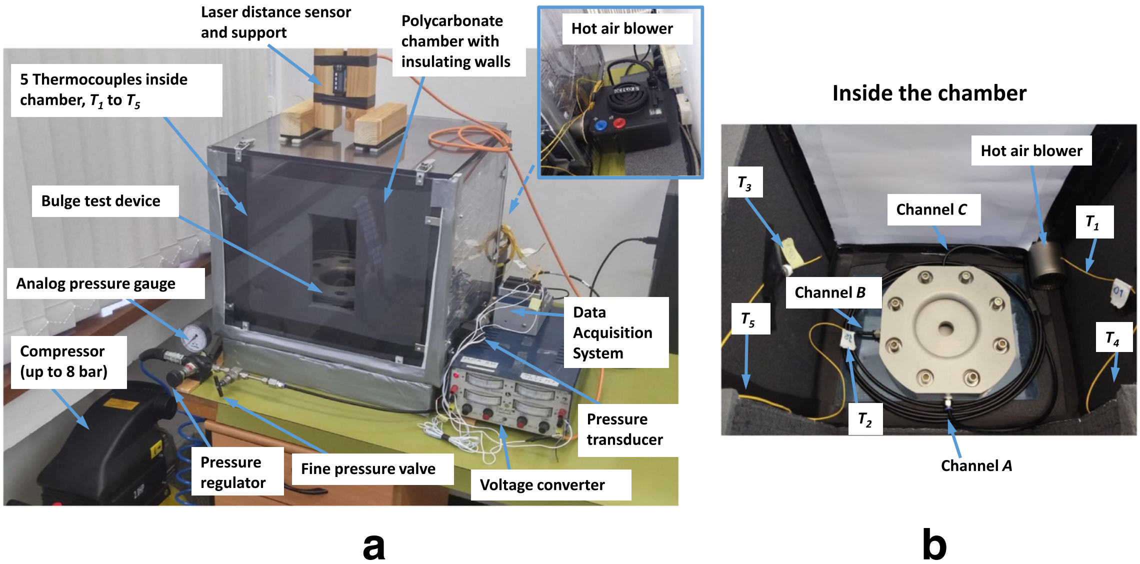

Fig. 2 Experimental setup

inside the bulge test device (through channel B), as shown in Fig. 2(b). When the required temperature is attained inside the chamber, compressed air is supplied through channel A from the bottom flange. Pressure is increased very slowly, to avoid viscous effects, by manually controlling the fine pressure valve. Pressure (P) inside the bulge test device is measured at channel C using a pressure transducer (range 0-4 bar with an accuracy of 0.5 %), which is calibrated against known values of pressure. During the inflation, vertical displacement of the center of the rubber specimen (δ) of the bulge test is measured using a low class number 2 laser displacement measurement sensor (range 150–1000 mm $\pm$ 0.5 mm on the max range. The max laser spot size of 3 mm $\times$ 6 mm has no local heating that may effect results. The initial state for which δ and P begin to measure is presented in Fig. 3. Clamping the rubber sheet between the top and middle aluminum flanges causes the formation of an initial cap which has the height of the top flange. All the measurements (temperature, pressure, and displacement) are recorded using a data acquisition card, and stored using a LabVIEW program.

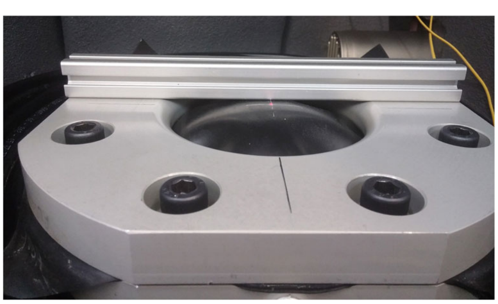

Fig. 3 Initial state of the bulge test

Remark It should be noted that standards don't define which exact experiments are needed in order to determine the mechanical properties of rubber materials. This is especially true for the case of ultimate deformation (strength) studies as reported in our work. Standard uni axial tests are usually interpreted in terms of small deformation theories. Such theories are inapplicable to rubber materials and soft materials in general.

Experiment Results

Bulge tests are performed for three different rubber materials namely (a) NBR, (b) Neoprene, and (c) Silicone. Average sheet thickness for NBR, Neoprene, and Silicone are about 1.2, 1.2 and 1.1 mm, respectively. For each rubber, tests are conducted under constant temperature environment at 4 different temperatures, 25 °C, 50 °C, 70 °C and 90 °C, comprising a total of 12 cases. The system including the bulge device and rubber specimen attached is exposed to preheating at the specified temperature for a period of no longer than half an hour. For each case, $P - \delta$ plots are shown in Figs. 4, 5 and 6 for NBR, Neoprene and Silicone, respectively. Each test is repeated several times (presented in different colors in Figs. 4 to 6 in order to ensure the repeatability and to obtain a representative behavior. The variation of the data is about $\pm 10\%$ due to slight variability in the specimens and loading rates. The average result is plotted as a black solid line. Failure points (P_u, δ_u) for the average results are marked with an open circle. The recorded temperatures show up to $\pm 3\%$ differences in values indicating the constant temperatures inside and outside the inflating balloon. Examples of

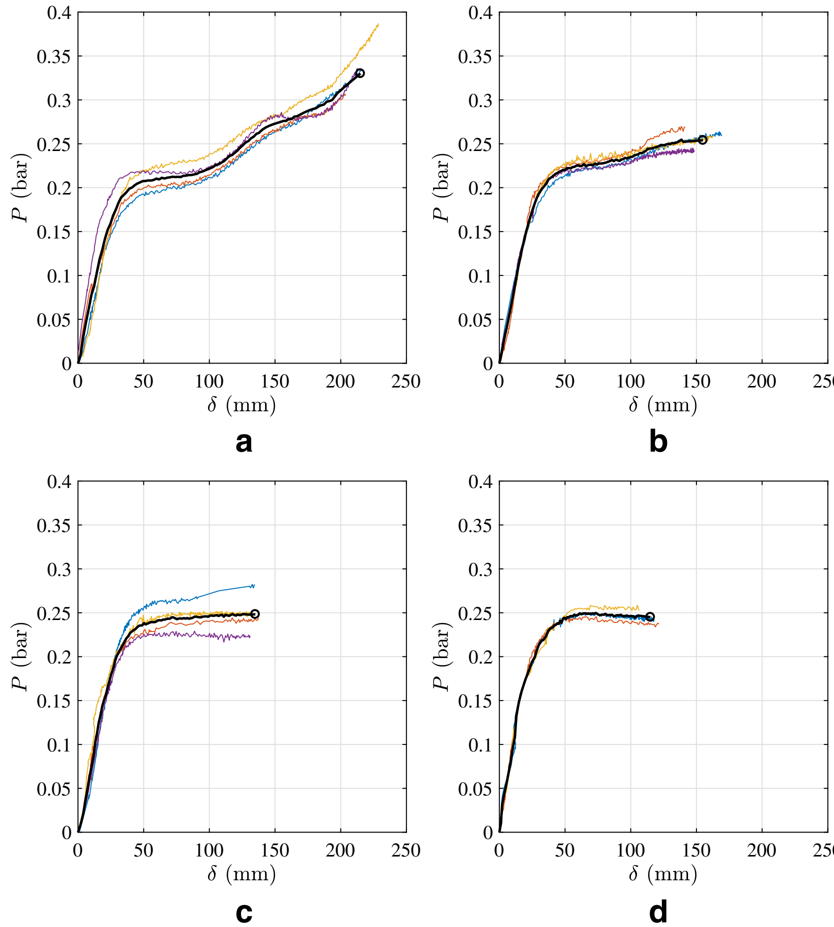

Fig. 4 Experimental $P-\delta$ curves for NBR at (**a**) 25 °C, (**b**) 50 °C, (**c**) 70 °C and (**d**) 90 °C. Average results are shown in black

recorded temperatures during 50 °C, 70 °C and 90 °C tests for NBR are presented in Fig. 7. It can be clearly observed that the ultimate vertical displacement of the pole (δ_u) decreases gradually with increasing temperature. This decrease is most significant in NBR, which is about 46%, as temperature increases from 25 °C to 90 °C. Neoprene shows about 26%, and Silicone being thermal resistant, shows only about 9% decrease in δ_u from 25 °C to 90 °C. The ultimate pressure (P_u) decreases as temperature increases from 25 °C to 50 °C. Further increase in temperature does not affect P_u significantly for all types of rubber materials. This initial decrease in P_u for NBR, Neoprene, and Silicone are about 23%, 25% and 15%, respectively. Some representative failure patterns are shown in Fig. 8. At room temperature (25 °C) cracks radiate in all directions from the pole due to the symmetry and isotropy of material, forming several fragments. Such cracks can be clearly seen in Fig. 8(a) and (b) for NBR and Neoprene, respectively. However, Silicone does not show this kind of pattern at room temperature and only a single fragment is observed (Fig. 8(c)). At higher temperatures the failure pattern changes from multiple fragments to a single kidney-shaped fragment for all kinds of rubber materials (Fig. 8(d)–(e)). The fracture line of the kidney-shaped fragments passes either through the pole or very near to the pole. These failure patterns suggest that the fracture would have occurred first at the pole (or near the pole), where the equi-biaxial condition exists. Small deviations of the fracture locations from the pole can be due to imperfections/inhomogeneities in the materials.

Finite Element Modeling of the Bulge Test

In order to characterize a material, an appropriate constitutive model needs to be calibrated with the test results obtained in "Experiment Results". In this section, we briefly present the constitutive model considered for modeling deformation and failure in rubber materials. Details of the FE model, which is used to simulate the bulge test are also presented.

Constitutive Model

For modeling of deformation and failure in rubber materials, we use the constitutive model by [18] which includes the

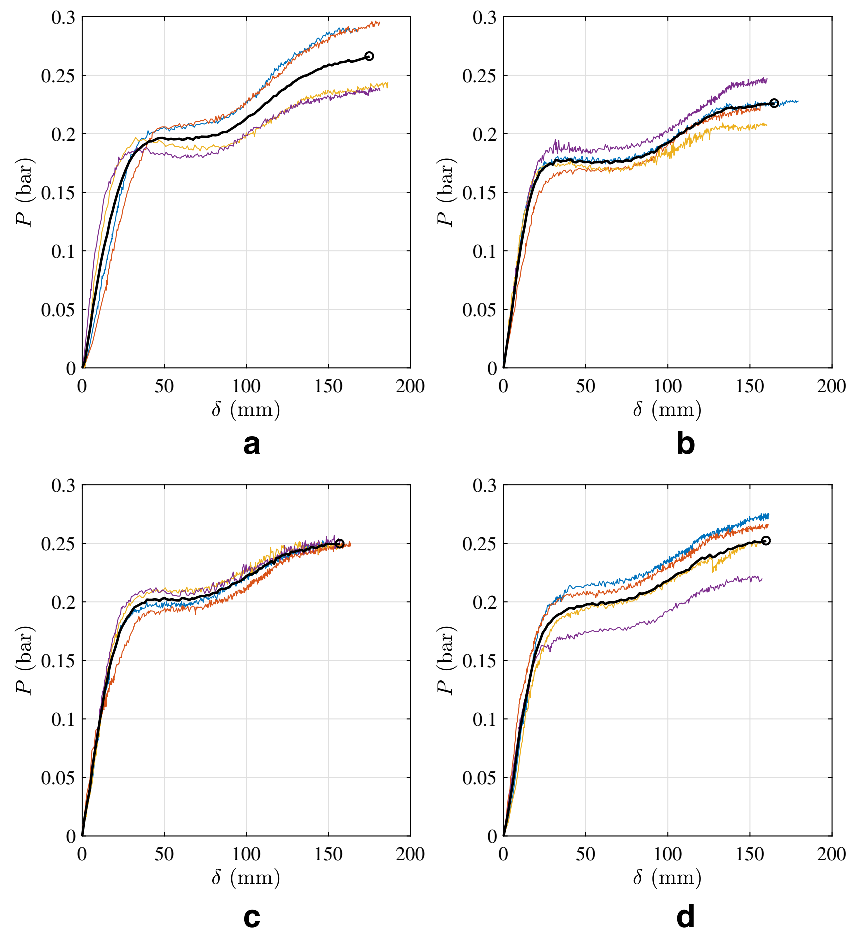

Fig. 5 Experimental $P-\delta$ curves for Silicone at (**a**) 25 °C, (**b**) 50 °C, (**c**) 70 °C and (**d**) 90 °C. Average results are shown in black

description of failure using energy limiters. For the detailed description of the theory of energy limiters, readers are referred to the series of articles by Volokh [18–21]. The basic idea of this simple approach is to introduce an energy limiter in the expression for strain energy function, which indicates the maximum amount of energy that can be stored and dissipated by the material volume during rupture. The limiter induces stress bounds in the constitutive equations automatically. The strain energy function ψ including the failure formulation, is given as,

$$\psi = \frac{\phi}{m}\left[\Gamma\left(\frac{1}{m},0\right) - \Gamma\left(\frac{1}{m},\frac{W^m}{\phi^m}\right)\right], \tag{1}$$

where ϕ is the energy limiter and m is a dimensionless parameter controlling the sharpness of transition to the material failure on the stress-strain curve. By increasing/decreasing m it is possible to simulate more/less steep ruptures of the internal bonds. W is the strain energy function of an intact material without failure. In the present case, W is considered as the Yeoh hyper-elastic model [22],

$$W = \sum_{k=1}^{3} c_k (I_1 - 3)^k, \tag{2}$$

where, c_k $(k = 1, 2, 3)$ are the material constants; I_1 is the first invariant of the left Cauchy strain tensor $\boldsymbol{b}$.

Assuming the incompressible condition where the Jacobin $J = 1$, the Cauchy stress is given as,

$$\boldsymbol{\sigma} = 2\boldsymbol{b}\frac{\partial\psi}{\partial\boldsymbol{b}} = 2\exp\left(-\frac{W^m}{\phi^m}\right)\frac{\partial W}{\partial I_1}\boldsymbol{b} - \kappa\boldsymbol{I}, \tag{3}$$

where κ is the Lagrange parameter to be obtained from boundary conditions. $\boldsymbol{I}$ is the second order identity tensor. It should be noted that for very large values of ϕ $(\phi \to \infty)$ equation (3) gives the stresses for the intact material (no failure). The almost constant failure pressure observed for tests done at 50 °C, 70 °C, and 90 °C (Figs. 4 to 6) are only due to the non-linear geometric behavior of the inflating balloon, which shows a region of increase in the vertical displacement while the pressure remains almost constant. On the other hand, the equal bi-axial stress that develops on the top (as plotted later in Figs. 12–14) continues to increase with the growing stretch.

In the bulge test configuration, the pole of the inflated sheet experiences equi-biaxial tensile state of stress and strain due to the axial symmetry. Stretches at the top

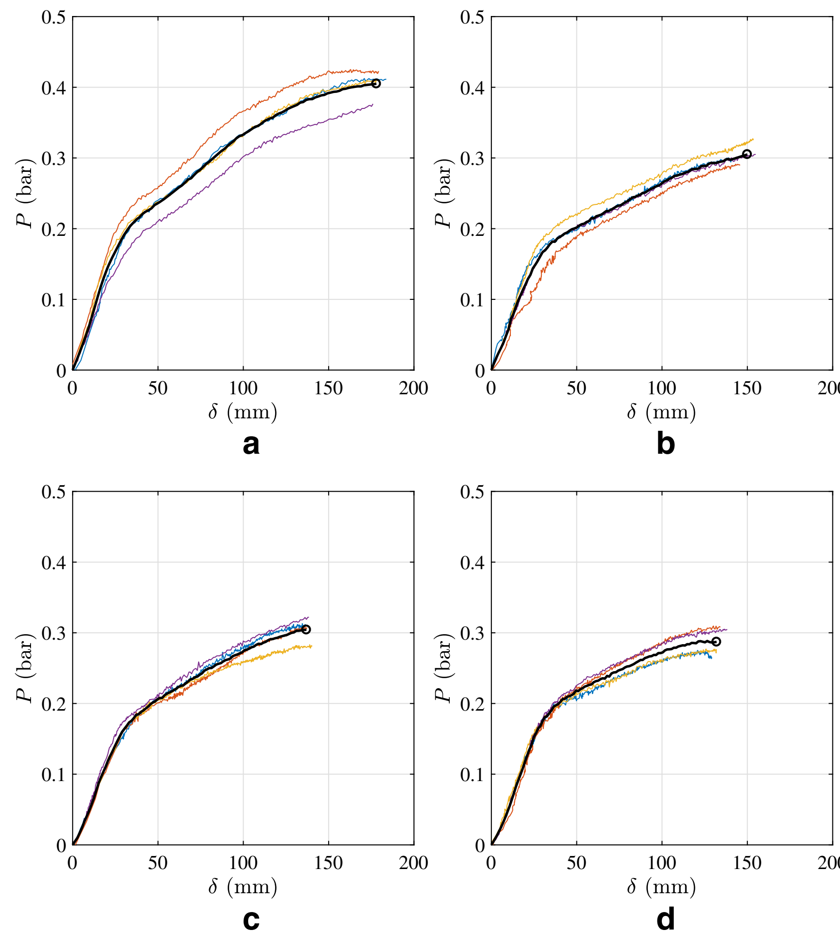

Fig. 6 Experimental $P-\delta$ curves for Neoprene at (**a**) 25 °C, (**b**) 50 °C, (**c**) 70 °C and (**d**) 90 °C. Average results are shown in black

(according to Fig. 9) are,

$$\lambda_1 = \lambda_2 = \lambda, \quad \lambda_3 = 1/\lambda^2. \tag{4}$$

Now, $\boldsymbol{b}$ becomes,

$$\boldsymbol{b} = \lambda^2 (\boldsymbol{e}_1 \otimes \boldsymbol{e}_1 + \boldsymbol{e}_2 \otimes \boldsymbol{e}_2) + 1/\lambda^4 \boldsymbol{e}_3 \otimes \boldsymbol{e}_3. \tag{5}$$

where $\boldsymbol{e}_i$ are standard Cartesian base vectors in deformed configuration.

Using equation (5) in (3), where κ is obtained by using the boundary condition $\sigma_3 = 0$, gives,

$$\sigma_1 = \sigma_2 = \sigma = 2\exp\left(-\frac{W^m}{\phi^m}\right)\left(\lambda^2 - \frac{1}{\lambda^4}\right) \times\left[c_1 + 2c_2\left(2\lambda^2 + \frac{1}{\lambda^4} - 3\right) + 3c_3\left(2\lambda^2 + \frac{1}{\lambda^4} - 3\right)^2\right]. \tag{6}$$

Equation (6) will be used in a later section to represent the equi-biaxial response of the different rubber materials.

Finite Element Model

FE simulations of the bulge experiments are performed in order to find the parameters of the constitutive model. Owing to the symmetry of loading as well as geometry about the central axis, the problem is analyzed as an axisymmetric shell, as shown schematically in Fig. 10. The vertical initial distance between point A and B is the top aluminum flange thickness (see Fig. 3). The Aluminum flange is modeled as a rigid surface. The rubber sheet is discretized using 3 noded axisymmetric shell elements. Frictional contact is provided between the outer rigid surface (flange) and the upper surface of shell elements (rubber sheet). The results were found to be insensitive to the coefficient of friction value. Parametric studies for the friction coefficient varying from 0.2 to 0.5, showed a difference of only about 3% in the maximum vertical displacement. The simulations are done with a coefficient of friction of 0.3. Pressure load is applied at the bottom surface of the shell elements. Symmetry boundary condition is applied at point A. All the translational degrees of freedom (DoFs) are constrained at point B. All DoFs at all the nodes of the rigid flange are constrained in all directions through

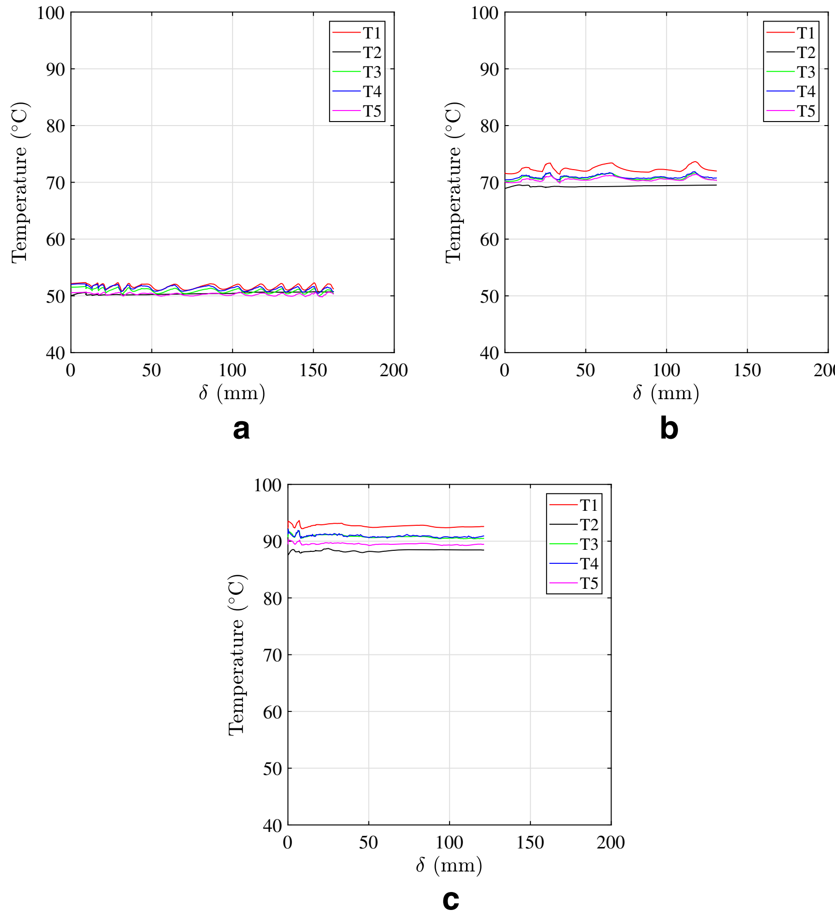

Fig. 7 Examples of recorded temperatures during (**a**) 50 °C, (**b**) 70 °C and (**c**) 90 °C tests for the NBR

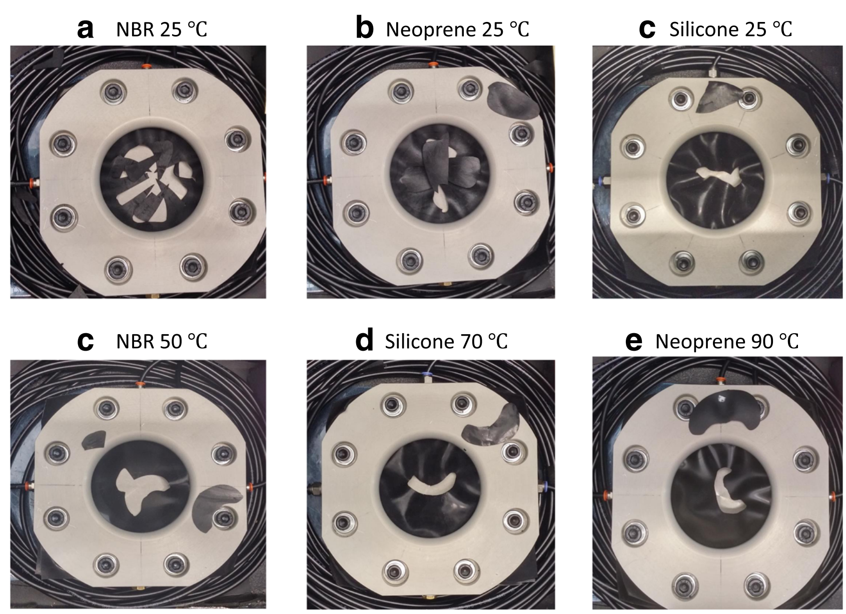

Fig. 8 Typical failure patterns for different cases. Separated fragments are also shown

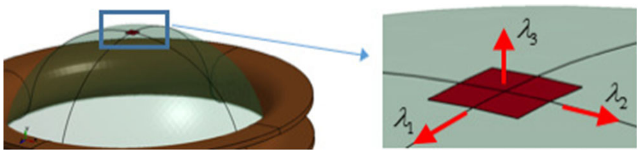

Fig. 9 Stretch directions at the pole of an inflated membrane

reference point C. The analysis done by ABAQUS v6.14 are implicit using quadrilateral shell elements. The mesh size is chosen according to a convergence check, where 2001 nodes and 1000 shell elements are used to obtain the solution. Maximum element size is 65 μm.

Calibration of the Constitutive Model

The constitutive model discussed in "Constitutive Model" is calibrated against the experimental results presented in "Experiment Results". The geometry of the specimen is modeled with close adherence to experimental conditions. Simulations are performed without modeling any material failure ($\phi \to \infty$) and the standard Yeoh model for hyperelastic material has been used for this purpose. Material constants (c_1, c_2, c_3) are varied following a heuristic approach. Appropriate constants are chosen based upon the best fit between the $P - \delta$ curves obtained from the experiments and simulations. Some representative comparisons for the $P - \delta$ curves are shown in Fig. 11 (one for each material and one for each temperature tested), and demonstrates the correlation achieved using the Yeoh model which contains three material parameters. Simulation results are plotted till $\delta = \delta_u$ for the corresponding experiment. Close match between the average $P - \delta$ plots from experiments and those from simulation are evident. Material parameters are chosen using the least squares minimization procedure to ensure that the overall deformation behavior is qualitatively captured. From simulations, stretches in meridional and hoop directions (λ_1 and λ_2) can be obtained. Both stretches λ_1 and λ_2 are found maximum (and same) for an

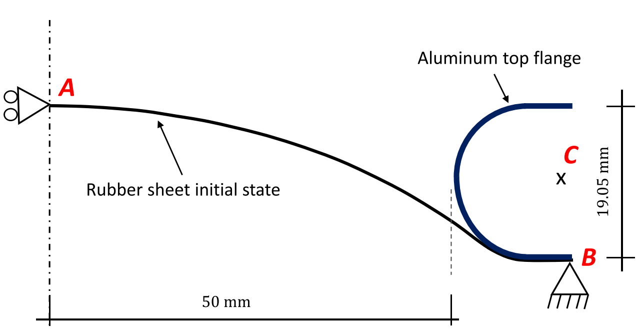

Fig. 10 Axisymmetric finite element model - Initial state

element near point A (see, Fig. 10), which confirms the possibility of fracture occurring first at the pole (or very near the pole in case of inhomogeneity) under equi-biaxial conditions during experiments. For this element, value of λ_1 (or λ_2) at $\delta = \delta_u$ provide failure stretch (λ_u) under equi-biaxial tension.

Knowing the failure stretch under equi-biaxial tension, we can now use equation (6) to find the corresponding energy limiter (ϕ). We consider "brittle" failure for which we choose $m = 10$. Further increase of this parameter does not affect results and the differences are negligible. [19]. Now, ϕ (the only unknown in equation (6)) can be obtained from the condition that the stress (σ) should be maximum when $\lambda = \lambda_u$, i.e.

$$\left.\frac{\partial \sigma}{\partial \lambda}\right|_{\lambda=\lambda_u} = 0. \tag{7}$$

For all cases, values of ϕ are obtained by solving equation (7). All parameters (c_1, c_2, c_3, ϕ) are shown in Tables 1, 2 and 3 for NBR, Neoprene and Silicone, respectively. For the range of temperature considered, it is observed that material behavior can be represented by almost constant material stiffness parameters (c_1, c_2, c_3) at all temperatures (except for Neoprene which is slightly stiffer at room temperature). However, energy limiter decreases with increasing temperature. For these parameters, the effect of temperature on the $\sigma - \lambda$ response under equi-biaxial tension from equation (6) and the corresponding material parameters, are presented in Figs. 12, 13 and 14 for NBR, Neoprene and Silicone, respectively. $\sigma - \lambda$ curves when no failure is considered ($\phi \to \infty$) are also plotted in red in Figs. 12–14. The assumption for $m = 10$ matches our observations in tests. While the experiment progresses slowly in a quasi-static manner the failure point is fast and sudden for all 3 materials tested. The small difference up to (σ_u) between the red curve representing no failure, and the blue curves which include the failure formulation, is a result of our assumption for the value of m. Table 4 summarizes all ultimate stretches (λ_u) and ultimate stresses (σ_u) found for each material and temperature tested. It can immediately be seen that the significant decrease in ultimate values, and energy limiters derived. For NBR and Neoprene, the ultimate stretch λ_u under equi-biaxial condition decreases significantly at the highest temperature considered by about 34% and 22%, respectively from its values at room temperatures. This results in a serious reduction in stress carrying capacity σ_u, which decreases 83% and 70% (compared to σ_u at room temperature) for NBR and Neoprene, respectively. For Silicone the decrease in λ_u and σ_u is only 5% and 24% accordingly because of the good thermal resistance. Here, it should be emphasized that the FE simulations discussed in

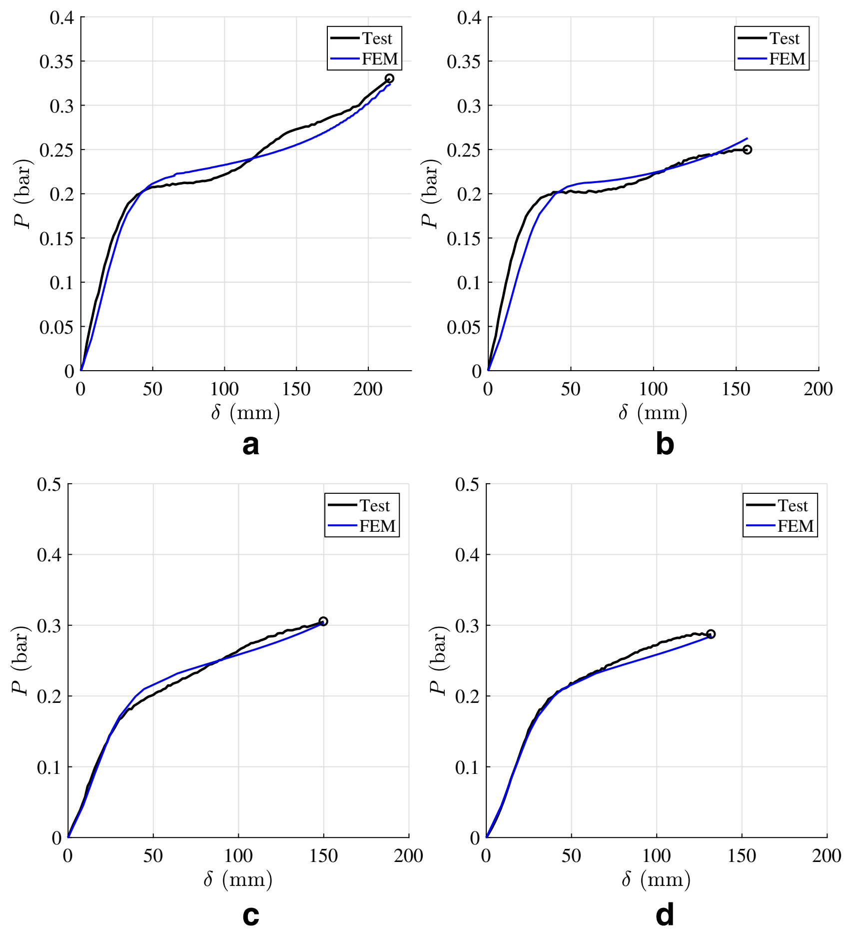

Fig. 11 Comparison of $P - \delta$ curves from experiments (average) and simulations for (**a**) NBR at 25 °C, (**b**) Silicone at 70 °C, (**c**) Neoprene at 50 °C and (**d**) Neoprene at 90 °C

"Finite Element Model" are performed with the Yeoh model without including any failure. Consideration of model with energy limiter in FE simulations to including failure will result in slightly lower pressure values than those shown in Fig. 11 near the failure point δ_u.

Now, we determine a new constitutive relation for the energy limiter, which allows to unify the description of the different materials. A suggestion including only one unit-less parameter, β, can be:

$$\phi = \phi_0 \left[exp(1 - T/T_0)\right]^{\beta}, \tag{8}$$

where T is temperature in Kelvin units (for which 25 °C is equal to 298.15 K). ϕ_0 and T_0 are ϕ and T at 25 °C accordingly. For each material, a β constant needs to be found. The values of β based upon the best fit between the test results of ϕ and the corresponding temperature are presented in Table 5. Figure 15 presents the test values of ϕ and T (marked with stars) as well as the resulting best fit curves derived from equation (8) and Table 5.

The 3 curves in Fig. 15 are the temperature related energy limiter for each material, which defines the value of ϕ in the strain energy ψ of equation (1).

Table 1 Material parameters for NBR

$c_1 = 0.22$ (MPa)
$c_2 = 2 \times 10^{-3}$ (MPa)
$c_3 = 4.5 \times 10^{-5}$ (MPa)

	25°C	50°C	70°C	90°C
ϕ (MPa)	51.1	20.7	15.7	11.6

Table 2 Material parameters for Neoprene

$c_1 = 0.22$ (MPa)
$c_2 = 3 \times 10^{-3}$ (MPa)
$c_3 = 7 \times 10^{-5}$ (MPa)

	25°C	50°C	70°C	90°C
ϕ (MPa)	40.0	20.5	16.6	15.3

Table 3 Material parameters for Silicone

$c_1 = 0.25$ (MPa)
$c_2 = 1 \times 10^{-5}$ (MPa)
$c_3 = 1 \times 10^{-4}$ (MPa)

	25°C	50°C	70°C	90°C
ϕ (MPa)	27.3	23.5	21.9	21.0

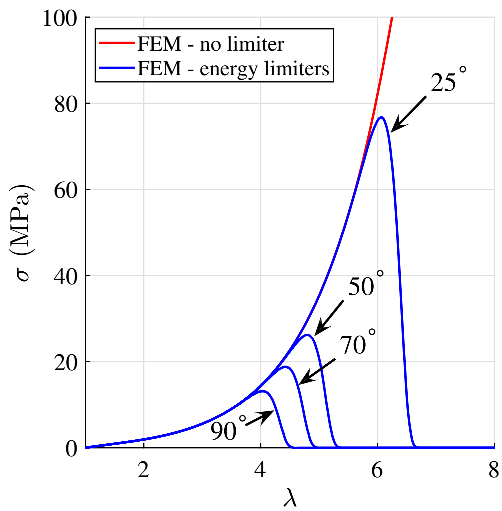

Fig. 12 $\sigma - \lambda$ curves for NBR under equi-biaxial tension at different temperature

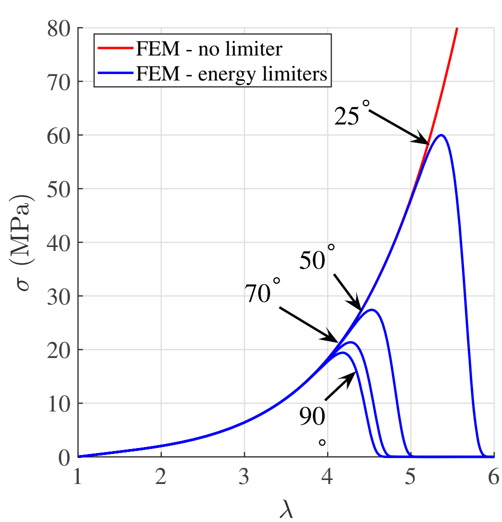

Fig. 13 $\sigma - \lambda$ curves for Neoprene under equi-biaxial tension at different temperature

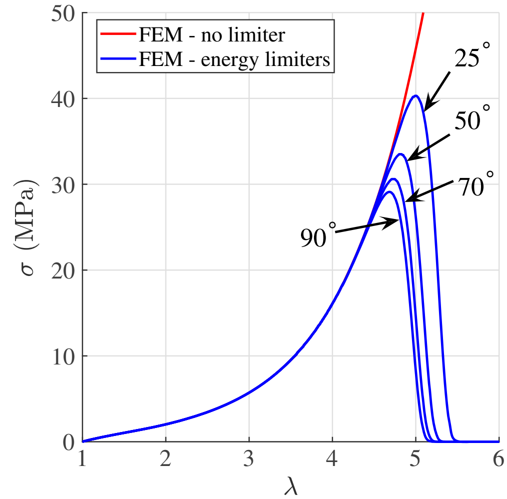

Fig. 14 $\sigma - \lambda$ curves for Silicone under equi-biaxial tension at different temperature

Table 4 Summary of ultimate biaxial properties

	NBR			Neoprene			Silicone		
	λ_u	σ_u (MPa)	ϕ (MPa)	λ_u	σ_u (MPa)	ϕ (MPa)	λ_u	σ_u (MPa)	ϕ (MPa)
25 °C	6.0	77	51.1	5.3	60	40.0	5.0	40	27.3
50 °C	4.8	26	20.7	4.5	27	20.5	4.8	34	23.5
70 °C	4.4	19	15.7	4.2	21	16.6	4.7	31	21.9
90 °C	4.0	13	11.6	4.1	19	15.3	4.7	29	21.0

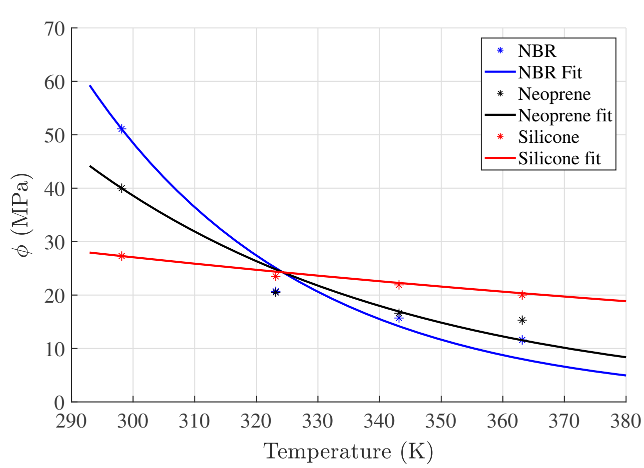

Fig. 15 Energy limiter as function of temperature. Scatter test values shown with star points at 25 °C, 50 °C, 70 °C, 90 °C, and continuous lines according to the limiter-temperature equation (equation (8)) for each material

Table 5 Values of the material parameter β (equation (8))

	NBR	Neoprene	Silicone
β	8.5	5.7	1.3

Conclusions

This work presents novel results on ultimate stress and stretch of rubber materials. The effect of short-term temperature on the ultimate stresses and stretch of rubber materials is absent in literature, which focuses mostly on the effect of temperature on the stiffness. Reaching ultimate properties at large stretches ($6 \sim 7$) while maintaining temperature control is difficult to perform in standard chambers. The method presented here uses the well established bulge test procedure with an additional design allowing temperature control also inside the inflating balloon. Tests conducted on three different rubber materials; NBR, Neoprene, and Silicone are presented. Since most practical applications of rubber membranes are subjected to bi-axial loading, it is most suitable to find the material parameters from a bulge test representing equal bi-axial conditions. Bulge tests are conducted under a constant temperature environment, at 4 different temperatures; 25 °C, 50 °C, 70 °C, 90 °C, and then simulated using the FE method. The constitutive model with energy limiters is used to include failure. Parameters of the constitutive model are obtained by comparison between experiments and simulations.

It is observed that material stiffness parameters are not significantly affected by temperature (for the range of temperatures tested). Ultimate properties σ_u and λ_u under bi-axial tension (and hence ϕ also) are significantly affected by the temperature. Even a small heat increase from 25 °C to 50 °C, results in a significant reduction in σ_u of 66% and 56% for NBR and Neoprene accordingly. σ_u and λ_u for Silicone rubber, which is known to have better thermal resistance compared to NBR and Neoprene rubber, is least affected by temperature, showing only a 13% decrease in σ_u for increase from 25 °C to 50 °C. The reason for the significant alterations in material failure properties is not clear. A possible clue to the explanation of the alterations could be found in the work by [11]. However, the latter work considers the influence of the long time exposure of rubber to thermal loads, while in our case it is a short time exposure. The issue should be clarified in future studies.

A new constitutive relation is suggested for the calibration of a more general thermoelastic energy limiter theory, assuming that an attached dependence of the limiter on the temperature exists. This allows the finding of ultimate properties as a function of high common operating temperatures for 3 commonly used rubber-like materials. The suggested model offers a new design consideration of the temperature related ultimate values.

Acknowledgments The support from the Israel Science Foundation (ISF-198/15) and the Israel Ministry of Construction is gratefully acknowledged. Authors also acknowledge help from Ofir Barak in preparing the LabVIEW interface for the experimental setup.

References

1. Epps JA (1994) Uses of recycled rubber tires in highways, vol 198. Transportation Research Board
2. Saccomandi G, Ogden RW (2004) Mechanics and thermomechanics of rubberlike solids, vol 452. Springer, Berlin
3. Anthony RL, Caston RH, Guth E (1942) Equations of state for natural and synthetic rubber-like materials. I. Unaccelerated natural soft rubber. J Phys Chem 46(8):826–840
4. Li X, Bai T, Li Z, Liu L (2016) Influence of the temperature on the hyper-elastic mechanical behavior of carbon black filled natural rubbers. Mech Mater 95:136–145
5. Lion A (1997) On the large deformation behaviour of reinforced rubber at different temperatures. J Mech Phys Solids 45(11):1805–1834
6. Rey T, Chagnon G, Le Cam JB, Favier D (2013) Influence of the temperature on the mechanical behaviour of filled and unfilled silicone rubbers. Polym Test 32(3):492–501
7. Treloar LRG (1975) The physics of rubber elasticity. Oxford University Press, Oxford
8. Gent A, Lindley P (1959) Internal rupture of bonded rubber cylinders in tension. Proc R Soc Lond A: Math Phys Eng Sci The Royal Society 249:195–205
9. Hamdi A, Abdelaziz MN, Hocine NA, Heuillet P, Benseddiq N (2006) A fracture criterion of rubber-like materials under plane stress conditions. Polym Test 25(8):994–1005
10. Marckmann G, Verron E (2006) Comparison of hyperelastic models for rubber-like materials. Rubber Chem Technol 79(5):835–858
11. Dickie RA, Smith TL (1969) Ultimate tensile properties of elastomers. VI. Strength and extensibility of a styrene–butadiene rubber vulcanizate in equal biaxial tension. J Polym Sci B Polym Phys 7(4):687–707
12. Charalambides MN, Wanigasooriya L, Williams GJ, Chakrabarti S (2002) Biaxial deformation of dough using the bubble inflation technique. I. Experimental. Rheol Acta 41(6):532–540
13. Fried I (1982) Finite element computation of large rubber membrane deformations. Int J Numer Methods Eng 18(5):653–660
14. Sasso M, Palmieri G, Chiappini G, Amodio D (2008) Characterization of hyperelastic rubber-like materials by biaxial and uniaxial stretching tests based on optical methods. Polym Test 27(8):995–1004
15. Coran A, Patel R (1980) Rubber-thermoplastic compositions. Part II. nbr-nylon thermoplastic elastomeric compositions. Rubber Chem Technol 53(4):781–794
16. Roeder CW, Stanton JF (1983) Elastomeric bearings: state-of-the-art. J Struct Eng 109(12):2853–2871
17. Rodgers B (2015) Rubber compounding: chemistry and applications, 2nd edn. CRC Press, Boca Raton
18. Volokh K (2007) Hyperelasticity with softening for modeling materials failure. J Mech Phys Solids 55(10):2237–2264

19. Volokh K (2010) On modeling failure of rubber-like materials. Mech Res Commun 37(8):684–689
20. Volokh K (2013) An approach to elastoplasticity at large deformations. Eur J Mech A Solids 39:153–162
21. Volokh K (2013) Review of the energy limiters approach to modeling failure of rubber. Rubber Chem Technol 86(3):470–487
22. Yeoh O (1990) Characterization of elastic properties of carbon-black-filled rubber vulcanizates. Rubber Chem Technol 63(5):792–805